Second-harmonic generation from spherical particles

Vera L. Brudny*
Facultad de Ciencias, Universidad Autónoma del Estado de Morelos, Av. Universidad 1001, 62210 Cuernavaca, Morelos, México

Bernardo S. Mendoza
Centro de Investigaciones en Optica, Apartado Postal 948-1, 37000 León, Guanajuato, México

W. Luis Mochán
Laboratorio de Cuernavaca, Instituto de Física, Universidad Nacional Autónoma de México, Apartado Postal 48-3, 62251 Cuernavaca, Morelos, México

(Received 30 May 2000)

We calculate the nonlinear dipole and quadrupole moments induced at the second-harmonic (SH) frequency 2ω in a small dielectric sphere by an inhomogeneous monochromatic electric field of frequency ω. We neglect finite-size effects and assume that the selvedge region of the sphere is thin enough so that the surface may be considered locally flat. The second-order dipole displays resonances corresponding to the excitation of dipolar and quadrupolar plasmons at ω and a dipolar plasmon at 2ω, besides the resonances in the nonlinear surface response parameters *a*, *b*, and *f*. The second-order quadrupole, on the other hand, has resonances corresponding to those of *a*, *b*, and *f*, and to the excitation of dipolar surface plasmons at ω only. Depending on the relation between the size of the sphere and the spatial scale of variation of the field, the SH radiation may be dominated by either dipolar or quadrupolar scattering, with a crossover region. As an application, we calculate the SH scattering of a Si sphere lying at various distances above a dielectric substrate.

I. INTRODUCTION

The use of nonlinear optical techniques to study surface phenomena has gained a lot of attention in recent years. In particular, second-harmonic generation (SHG) has been established as a very powerful spectroscopy to study a wide range of physical and chemical phenomena at the surface of centrosymmetric materials.[1–7] The surface sensitivity of SHG is due to the fact that within the dipole approximation a centrosymmetric environment does not radiate SH, while the inversion symmetry is broken at its surface, thus allowing the radiation of SH. On the experimental side, the new tunable high intensity laser systems have made SHG spectroscopy readily accessible and applicable to a wide range of systems.[1–7] However, the theoretical development of the field is still an ongoing subject of research. Some recent advances for the case of semiconducting and metallic systems have appeared in the literature, where the confrontation of theoretical models with experiment has succeeded, yielding correct physical interpretations for the SHG spectra.[8–13] Most of the SHG studies, both theoretical and experimental, have been concerned with planar surfaces, and much less attention has been paid to nonplanar systems. Novel nanofabrication techniques are now capable of producing nanoparticles with controlled structures which include small clusters, self-assembled particles, quantum dots, vesicles, etc. The nonlinear optical properties of these structures are important for applications, and can be used for their physical characterization.[14]

There have been few theoretical investigations dealing with the SH behavior of small spheres. Most of them make use of very restrictive models for the intrinsic bulk[15,16] or surface[17,18] nonlinear optical response of the sphere. The centrosymmetry of a nanoparticle is locally disrupted by its surface. However, it is regained globally for a spherical shape. Thus, a homogeneous polarizing field induces mutually canceling polarizations at opposite sides of the sphere, and would be incapable of producing dipolar radiation; it would produce only higher multipolar radiation with a power of leading order k^6, where k is the wave number. However, for a nonuniform polarizing field, this cancellation is no longer exact and dipolar radiation becomes possible. Recently Dadap *et al.*[19,20] presented a model that permits an arbitrary nonlinear intrinsic response, and calculated the second-harmonic (SH) Rayleigh scattering from a small sphere of centrosymmetric material illuminated by a linearly or circularly polarized plane wave. Retardation of the incoming field across the particle leads to a total dipole moment that scales as R/λ for small spheres, where R is the radius of the sphere and λ the wavelength. Thus, although retardation leads to dipolar radiation, it is of order k^6, and therefore comparable to the quadrupolar radiation, instead of the usual linear dipolar Mie scattering which is of order k^4 and dominates over the quadrupolar scattering.

The field variations of a plane wave due to retardation take place necessarily along its wave vector, which is perpendicular to the polarizing field, and with a concomitant length scale λ. However, in many systems of interest, such as in the neighborhood of other particles or of a substrate, the field may have variations with other length scales and along different directions. Since for small length scales the polarizing field is mostly longitudinal, our purpose in this paper is the full calculation of the SHG by a small spherical particle subject to an inhomogeneous longitudinal field. To this end, we extend the *continuous dipolium* model developed originally to obtain SHG and the sum and/or difference frequency

generation (SFG/DFG) for a semiinfinite homogeneous isotropic dielectric.[21,22] This model allowed a closed analytical solution for the surface and bulk nonlinear susceptibilities in terms of the linear dielectric function of the system. Here, we consider a particle of radius $R \ll \lambda$ but large enough so that we may assume those results to be locally valid inside and at the surface of the sphere. Thus, we obtain simple analytical expressions for the dipolar and quadrupolar nonlinear susceptibilities of the sphere. Their use permits a detailed analysis of the spectral features of the SHG radiated power and of the radiation patterns. As a realistic application, we analyze the SHG of a Si nanosphere placed above an inert dielectric substrate.

The structure of the paper is the following: In Sec. II we develop the theory for the nonlinear response of an isolated single sphere and its SHG efficiency. In Sec. III we use these results to calculate the response of a sphere placed above a semiinfinite inert dielectric substrate with a flat surface, interacting at the fundamental and SH frequencies with its own dipole and quadrupole image fields. In Sec. IV we obtain numerical results for the SH radiation by a simple system with a single Lorentzian linear resonance and identify the origin of all the spectral features (Sec. IV A). We then study in detail the radiation of a Si nanosphere above an inert substrate (Sec. IV B). Finally, Sec. V is devoted to conclusions.

II. NONLINEAR RESPONSE OF A SINGLE SPHERE

We first consider a small polarizable sphere of radius R centered at the origin and subject to an inhomogeneous polarizing external field $\vec{E}^{\rm ex}(\vec{r})$ which oscillates at frequency ω. Due to the overall centrosymmetry of the system, its quadratic dipole moment $\vec{p}$ has no *local* contribution proportional to $\vec{E}^{\rm ex}\vec{E}^{\rm ex}$. Thus, $\vec{p}$ is a *nonlocal* quantity which depends on the spatial variation of the field and can be written as $\vec{p} \propto \vec{E}^{\rm ex}(0)\nabla\vec{E}^{\rm ex}(0) + \cdots$, where we only keep the lowest-order spatial derivatives. Due to the spherical symmetry of the system, we write[23]

$$\vec{p} = \gamma^d(\omega)\vec{E}^{\rm ex}(0)\cdot\nabla\vec{E}^{\rm ex}(0), \tag{1}$$

where γ^d is a scalar. Here, we have ignored a contribution proportional to $k_1\vec{E}^{\rm ex}\times\vec{B}^{\rm ex}$ since we are neglecting retardation, i.e., we assume $|\nabla E^{\rm ex}| \gg B^{\rm ex}/\lambda_1$, where $\vec{B}^{\rm ex}$ is the external magnetic field, $\lambda_1 = 2\pi/k_1$ the fundamental wavelength, and $k_m = m\omega/c$ the free-space wave number of the mth harmonic ($m = 1,2$). We have also dropped a third contribution compatible with spherical symmetry, proportional to $\vec{E}^{\rm ex}\nabla\cdot\vec{E}^{\rm ex}$, assuming no external charges within the sphere. Similarly, the quadrupole moment of the sphere $\vec{\vec{Q}} \propto \vec{E}^{\rm ex}(0)\vec{E}^{\rm ex}(0)$ may be written as

$$Q_{ij} = \gamma^Q(\omega)[E_i^{\rm ex}(0)E_j^{\rm ex}(0) - \tfrac{1}{3}\delta_{ij}(E^{\rm ex}(0))^2]. \tag{2}$$

The purpose of this section is the calculation of the nonlinear dipolar and quadrupolar polarizabilities γ^d and γ^Q.

We describe the fundamental field close to the sphere by a scalar potential

$$\phi^{\rm ex}(r,\theta,\varphi) = \sum_{lm} A_{lm} r^l Y_{lm}(\theta,\varphi), \tag{3}$$

where r, θ, and φ are spherical coordinates and Y_{lm} are spherical harmonics. For our purposes, it is enough to restrict our attention to a simple, cylindrically symmetric linearly varying field,

$$\phi^{\rm ex} = A_{10} r Y_{10} + A_{20} r^2 Y_{20}. \tag{4}$$

In this case, we identify

$$\vec{E}^{\rm ex} = -\sqrt{\frac{3}{4\pi}} A_{10}\hat{z}, \tag{5}$$

and

$$\vec{E}^{\rm ex}(0)\cdot\nabla\vec{E}^{\rm ex}(0) = \frac{\sqrt{15}}{2\pi} A_{10}A_{20}\hat{z}. \tag{6}$$

Consistently with Eqs. (1) and (2), in the following results we only keep nonlinear terms proportional to A_{10}^2 and $A_{10}A_{20}$, and drop all others.

Solving Laplace's equation and imposing boundary conditions at $r = 0$, R, and ∞ yields the self-consistent linear potential

$$\phi_1 = \begin{cases} A_{10}\left[1 - \dfrac{\epsilon_1 - 1}{\epsilon_1 + 2}\left(\dfrac{R}{r}\right)^3\right] r Y_{10} + A_{20}\left[1 - 2\dfrac{\epsilon_1 - 1}{2\epsilon_1 + 3}\left(\dfrac{R}{r}\right)^5\right] r^2 Y_{20}, & r > R \\ A_{10}\dfrac{3}{\epsilon_1 + 2} r Y_{10} + A_{20}\dfrac{5}{2\epsilon_1 + 3} r^2 Y_{20}, & r < R, \end{cases} \tag{7}$$

where $\epsilon_m \equiv \epsilon(m\omega)$ is the dielectric function at the mth harmonic.

Following Ref. 21, this inhomogeneous potential induces a nonlinear macroscopic polarization

$$\vec{P}^{\rm nl} = n\vec{p}^{\rm nl} - \frac{1}{2} n\nabla\cdot\vec{q}^{\rm nl} \tag{8}$$

within the sphere, where n is the number density of the polarizable entities (''molecules'') that make up the system,

$$\vec{p}^{\rm nl} = -\frac{1}{2e}\alpha_1\alpha_2\nabla E_1^2 \tag{9}$$

is the nonlinear dipole moment of a single molecule,

$$\vec{q}^{\,\mathrm{nl}} = -\frac{1}{e}\alpha_1^2 \vec{E}_1 \vec{E}_1 \tag{10}$$

is the second moment of the induced molecular charge, closely related to its quadrupole moment[24] $Q_{ij}^{\mathrm{nl}} = 3q_{ij}^{\mathrm{nl}} - \delta_{ij} q_{kk}^{\mathrm{nl}}$, $\alpha_m \equiv \alpha(m\omega)$ is the linear molecular polarizability related to the dielectric function by $\epsilon_m = 1 + 4\pi n \alpha_m$, $-e$ is the charge of an electron, and $\vec{E}_1 = -\nabla \phi_1$ is the driving linear field.

The macroscopic polarization (8) yields a nonlinear charge density $\rho^{\mathrm{nl}} = -\nabla \cdot \vec{P}^{\mathrm{nl}}$. For our linearly varying fundamental field,

$$\rho^{\mathrm{nl}} = -\frac{375n}{4\pi e}\frac{\alpha_1(\alpha_1 - 2\alpha_2)}{(3+2\epsilon_1)^2} A_{20}^2 \tag{11}$$

turns out to be independent of $\vec{r}$ and proportional to $|\nabla E^{\mathrm{ex}}|^2$, and therefore negligible.

Now we turn our attention to the surface of the sphere. There, we find a bulk originated nonlinear surface charge $\sigma^{\mathrm{nl}\,b} = \vec{P}^{\mathrm{nl}}(R^-) \cdot \hat{r}$ due to the termination of the bulk nonlinear polarization, where $\hat{r}$ is a radial unit vector and $R^{\pm}$ denote the outer and/or inner side of the surface. We obtain

$$\sigma^{\mathrm{nl}\,b} = \frac{5n}{16\pi e}\alpha_1(\alpha_1 - 2\alpha_2)\left(\frac{12\sqrt{15}\cos\theta}{(\epsilon+2)(2\epsilon+3)} A_{10}A_{20} + 25\frac{(3\cos 2\theta + 5)}{(2\epsilon+3)^2} R A_{20}^2 \right), \tag{12}$$

from which we need only keep the first term. Notice that only the second term contributes to the total charge at the surface, which, as expected, is canceled by the bulk charge. We remark that Eqs. (11) and (12) contain the contributions from the bulk quadrupole moment density and its truncation at the surface.

There is also a ''surface-originated'' surface charge

$$\sigma^s = -\nabla_{\parallel} \cdot \vec{P}_{\parallel}^{\,s}, \tag{13}$$

where $\vec{P}_{\parallel}^{\,s}$ is the projection of the surface nonlinear polarization onto the surface of the sphere and $\nabla_{\parallel}$ denotes the gradient operator along the surface. Since the centrosymmetry is locally broken close to the surface of the sphere, we consider a surface nonlinear polarization of a dipolar form, namely,

$$P_i^s = \chi_{ijk}^s F_j F_k. \tag{14}$$

Here, $\vec{\vec{\chi}}^{\,s}$ denotes the local nonlinear susceptibility of the surface, defined as the response to the field $\vec{F} = (\vec{D}_1(R))_{\perp} + (\vec{E}_1(R))_{\parallel}$, made up of the normal projection ($\perp$) of the displacement field and the parallel projection ($\parallel$) of the linear electric field evaluated at the surface. Defining the surface response in this way, i.e., in terms of quantities that are continuous across the surface, eliminates the ambiguities as to where in the selvedge the fields should be evaluated. In our case, $\vec{F} = \vec{E}_1(R^+) = \epsilon_1(\vec{E}_1(R^-))_{\perp} + (\vec{E}_1(R^-))_{\parallel}$.

Now, we assume that the width of the selvedge is small compared to R and we neglect finite-size effects, so that $\vec{\vec{\chi}}^{\,s}$ is given *locally* by the response of a flat semiinfinite system. Thus, if we consider a local reference frame in which the outgoing radial direction $\perp$ is along one of the Cartesian axis, we may write the surface nonlinear susceptibility of an isotropic material as

$$\chi_{ijk}^s = \frac{(\epsilon_1 - 1)^2}{64\pi^2 ne}\left(\delta_{i\perp}\delta_{j\perp}\delta_{k\perp}\frac{a}{\epsilon_1^2} + [(1-\delta_{i\perp})(1-\delta_{j\perp})\delta_{k\perp} + (1-\delta_{i\perp})\delta_{j\perp}(1-\delta_{k\perp})]\frac{b}{\epsilon_1} + \delta_{i\perp}(1-\delta_{j\perp})(1-\delta_{k\perp})f \right), \tag{15}$$

where $a = a(\omega)$, $b = b(\omega)$, and $f = f(\omega)$ are dimensionless functions which are commonly employed to parametrize the response of the surface.[25]

Substituting Eq. (15) into Eq. (13) yields

$$\sigma^s = \frac{3(\epsilon_1 - 1)^2 b}{256ne\pi^3 R}\left(9\frac{(1+3\cos 2\theta)}{(\epsilon_1+2)^2} A_{10}^2 + 20\sqrt{15}R\frac{2\cos\theta + 3\cos 3\theta}{(\epsilon_1+2)(2\epsilon_1+3)} A_{10}A_{20} + \ldots \right), \tag{16}$$

where, as discussed above, we have omitted a term proportional to A_{20}^2. Finally, we also write down the surface polarization normal to the surface,

$$P_{\perp}^s = \frac{(\epsilon_1 - 1)^2}{256ne\pi^3}\left(27\frac{a\cos^2\theta + f\sin^2\theta}{(\epsilon_1+2)^2} A_{10}^2 + 15\sqrt{15}R\cos\theta\frac{4a + 6(f-a)\sin^2\theta}{(\epsilon_1+2)(2\epsilon_1+3)} A_{10}A_{20} + \ldots \right). \tag{17}$$

We now consider the potential $\phi_2 = \phi(2\omega)$ induced in the system at the second-harmonic frequency. Notice that ρ^{nl} [Eq. (11)] and $\sigma^{\mathrm{nl}\,b}$ [Eq. (12)] play the role of external sources for ϕ_2 and have to be screened by the linear response of the system ϵ_2, while σ^s [Eq. (16)] and $P_{\perp}^s$ [Eq. (17)] are self-consistent in the sense of being already screened by the surface response. Thus, it is convenient to separate

$$\phi_2 = \phi^b + \phi^s, \tag{18}$$

where ϕ^b is produced by the unscreened bulk originated sources and ϕ^s is due to the screened surface contributions. The equations to be solved are thus

$$\nabla^2 \phi^b = \begin{cases} -4\pi\rho^{\mathrm{nl}}/\epsilon_2 & (\text{inside}) \\ 0 & (\text{outside}) \end{cases} \tag{19}$$

and

$$\nabla^2 \phi^s = 0 \quad (\text{inside and outside}) \tag{20}$$

with boundary conditions

$$\phi^b(R^+) - \phi^b(R^-) = 0, \tag{21}$$

$$\phi^s(R^+)-\phi^s(R^-)=4\pi P_\perp^s, \tag{22}$$

$$\frac{\partial}{\partial R}\phi^b(R^+)-\epsilon_2\frac{\partial}{\partial R}\phi^b(R^-)=-4\pi\sigma^b, \tag{23}$$

and

$$\frac{\partial}{\partial R}\phi^s(R^+)-\frac{\partial}{\partial R}\phi^s(R^-)=-4\pi\sigma^s. \tag{24}$$

Expanding the potentials $\phi^\lambda(\vec{r})=\Sigma_{lm}\phi_{lm}^\lambda(r)Y_{lm}(\theta,\varphi)$ $(\lambda=s,b)$ and their sources $s(\theta,\varphi)=\Sigma_{lm}s_{lm}Y_{lm}(\theta,\varphi)$ $(s=\sigma^{\mathrm{nl}\,b},\sigma^s,P_\perp^s)$ in spherical harmonics, we obtain

$$\phi_{l0}^\lambda=\begin{cases} F_{l0}^\lambda r^l & \text{(inside)} \\ \dfrac{4\pi}{2l+1}\dfrac{q_{l0}^\lambda}{r^{l+1}} & \text{(outside)} \end{cases} \tag{25}$$

for $l\geqslant 1$, and the boundary conditions become

$$\frac{4\pi}{2l+1}\frac{q_{l0}^b}{R^{l+1}}-F_{l0}^bR^l=0, \tag{26}$$

$$\frac{4\pi}{2l+1}\frac{q_{l0}^s}{R^{l+1}}-F_{l0}^sR^l=4\pi(P_\perp^s)_{l0}, \tag{27}$$

$$4\pi\frac{l+1}{2l+1}\frac{q_{l0}^b}{R^{l+2}}-\epsilon_2 lF_{l0}^bR^{l-1}=-4\pi\sigma_{l0}^{\mathrm{nl}\,b}, \tag{28}$$

$$4\pi\frac{l+1}{2l+1}\frac{q_{l0}^s}{R^{l+2}}-lF_{l0}^sR^{l-1}=-4\pi\sigma_{l0}^s. \tag{29}$$

The solutions of this system yield the potential amplitudes F_{lm}^λ inside, and the nonlinear (screened, self-consistent) spherical multipole moments induced on the sphere $q_{l0}=q_{l0}^b+q_{l0}^s$, with

$$q_{l0}^b=\frac{2l+1}{l\epsilon_2+l+1}R^{l+2}\sigma_{l0}^{\mathrm{nl}\,b} \tag{30}$$

and

$$q_{l0}^s=lR^{l+1}(P_\perp^s)_{l0}+R^{l+2}\sigma_{l0}^s. \tag{31}$$

We have skipped the analysis of the monopolar $l=0$ fields, since the sphere remains globally neutral.

From Eqs. (12) and (16) we have

$$\sigma_{10}^{\mathrm{nl}\,b}=\frac{15}{32\pi^2ne}\sqrt{\frac{5}{\pi}}\frac{(\epsilon_1-1)(\epsilon_1-2\epsilon_2+1)}{(\epsilon_1+2)(2\epsilon_1+3)}A_{10}A_{20}, \tag{32}$$

$$\sigma_{10}^s=\frac{3}{32\pi^2ne}\sqrt{\frac{5}{\pi}}\frac{(\epsilon_1-1)^2}{(\epsilon_1+2)(2\epsilon_1+3)}bA_{10}A_{20}, \tag{33}$$

$$\sigma_{20}^s=\frac{27}{32\pi^2ne}\frac{1}{\sqrt{5\pi}}\frac{(\epsilon_1-1)^2}{(\epsilon_1+2)^2}\frac{b}{R}A_{10}^2+\cdots, \tag{34}$$

$$(P_\perp^s)_{10}=\frac{3}{32\pi^2ne}\sqrt{\frac{5}{\pi}}\frac{(\epsilon_1-1)^2}{(\epsilon_1+2)(2\epsilon_1+3)}(2a+3f)RA_{10}A_{20}, \tag{35}$$

and

$$(P_\perp^s)_{20}=\frac{9}{64\pi^2ne}\frac{1}{\sqrt{5\pi}}\frac{(\epsilon_1-1)^2}{(\epsilon_1+2)^2}(a-f)A_{10}^2+\cdots, \tag{36}$$

which yield

$$q_{10}^b=\frac{45}{32\pi^2ne}\sqrt{\frac{5}{\pi}}\frac{(\epsilon_1-1)(\epsilon_1-2\epsilon_2+1)}{(\epsilon_1+2)(2\epsilon_1+3)(\epsilon_2+2)}R^3A_{10}A_{20}, \tag{37}$$

$$q_{10}^s=\frac{3}{32\pi^2ne}\sqrt{\frac{5}{\pi}}\frac{(\epsilon_1-1)^2}{(\epsilon_1+2)(2\epsilon_1+3)}\times(2a+b+3f)R^3A_{10}A_{20}, \tag{38}$$

$$q_{20}^s=\frac{9}{32\pi^2ne}\frac{1}{\sqrt{5\pi}}\frac{(\epsilon_1-1)^2}{(\epsilon_1+2)^2}(a+3b-f)R^3A_{10}^2+\cdots, \tag{39}$$

where we have neglected terms of order A_{20}^2 and multipolar moments that go to zero faster than R^3 as $R\to 0$.

Finally, we identify the Cartesian components of the dipole and quadrupole moments $p_z=\sqrt{4\pi/3}q_{10}$ and $Q_{zz}=2\sqrt{4\pi/5}q_{20}$ and employ Eqs. (1), (2), (5), and (6) to write down the dipolar and quadrupolar nonlinear polarizabilities

$$\gamma^d=\frac{1}{8\pi ne}\frac{\epsilon_1-1}{(\epsilon_1+2)(2\epsilon_1+3)}\left(15\frac{\epsilon_1-2\epsilon_2+1}{\epsilon_2+2}+(\epsilon_1-1)(2a+b+3f)\right)R^3, \tag{40}$$

and

$$\gamma^Q=\frac{9}{20\pi ne}\frac{(\epsilon_1-1)^2}{(\epsilon_1+2)^2}(a+3b-f)R^3. \tag{41}$$

One can identify bulk and surface contributions to γ^d, the latter being proportional to the surface parameters *a*, *b*, and *f*. It is interesting to note that *both* contributions scale with the volume of the sphere and not with its area. Although σ^s has a term $\propto 1/R$ [Eq. (16)] and $P_\perp^s$ has a term independent of R [Eq. (17)], both of which could have contributed to a dipole moment $\propto R^2$, these contributions are canceled out due to the overall centrosymmetry of the sphere. The surface contribution to γ^d inherits the resonant structure of *a*, *b*, and *f*, while its bulk contribution has resonances at frequencies for which the second-harmonic depolarization field excites a dipolar plasmon, given by the condition $\epsilon_2=-2$. There are further resonances in both terms corresponding to the excitation of dipolar and quadrupolar plasmons at the fundamental frequency, given by the conditions $\epsilon_1=-2$ and $\epsilon_1=-3/2$, respectively.

The quadrupolar response [Eq. (41)] also scales with the volume of the sphere. It may seem paradoxical that it con-

tains only a ''surface'' term, since each ''molecule'' within the sphere has a finite quadrupole moment [Eq. (10)]. The reason is that a, b, and f necessarily contain bulk contributions besides intrinsic surface contributions,[26] so that the bulk quadrupolar contribution is actually present but hidden within the ''surface contribution.'' Besides the resonances of the surface parameters, γ^Q has only a dipolar (double) resonance at the fundamental frequency.

Finally, the radiated electromagnetic field at 2ω may be calculated from

$$\vec{B}_2 = k_2^2 \hat{n} \times \vec{p}^{\,\mathrm{ef}} \frac{e^{ik_2 r}}{r}, \tag{42}$$

$$\vec{E}_2 = \vec{B}_2 \times \hat{n}, \tag{43}$$

where $\hat{n}$ is a unit vector in the direction of observation and the effective dipole moment is given by

$$p_i^{\mathrm{ef}} = \left(p_i - \frac{i}{6} k_2 Q_{ij} \hat{n}_j \right) = \left[\gamma^d E_j^{\mathrm{ex}} \partial_j E_i^{\mathrm{ex}} - \frac{i}{6} k_2 \gamma^Q \left(E_i^{\mathrm{ex}} E_j^{\mathrm{ex}} \hat{n}_j - \frac{1}{3} E_k^{\mathrm{ex}} E_k^{\mathrm{ex}} \hat{n}_i \right) \right]. \tag{44}$$

Equations (42) and (43) contain both the electric dipole and quadrupole fields. These contributions might be comparable or one might dominate over the other, depending on the size of the field gradient. The SH power radiated per unit solid angle is

$$\frac{d\mathcal{P}}{d\Omega} = \frac{c}{8\pi} k_2^4 |(\hat{n} \times \vec{p}^{\,\mathrm{ef}}) \times \hat{n}|^2. \tag{45}$$

The SH power is proportional to I_1^2, where $I_1 = (c/8\pi)|E^{\mathrm{ex}}|^2$ is the intensity of a plane wave with amplitude $\vec{E}^{\mathrm{ex}}$, so that, in analogy to the definition of the linear scattering cross section, we define a nonlinear differential efficiency as

$$\frac{d\sigma}{d\Omega} \equiv \frac{1}{I_1^2} \frac{d\mathcal{P}}{d\Omega} = \frac{8\pi}{c} k_2^4 \frac{|(\hat{n} \times \vec{p}^{\,\mathrm{ef}}) \times \hat{n}|^2}{|E^{\mathrm{ex}}|^4} \tag{46}$$

with units $[\sigma] = \mathrm{cm}^4/W$. Out of resonance, we expect σ to be of order between $(k_2 R)^4 (R/l)^2/(cn^2 e^2)$ for dipole-dominated and $(k_2 R)^6/(cn^2 e^2)$ for quadrupole-dominated radiation, where l is the length scale of the field spatial variation.

III. NONLINEAR RESPONSE OF A SPHERE ABOVE A SUBSTRATE

In the preceding section we have obtained the SH nonlinear dipole and quadrupole moments induced on a small sphere by an applied inhomogeneous field. Our derivation assumes that the field gradient is large enough so that retardation effects may be neglected, but small enough so that only terms of first order in the field derivatives need to be kept. Thus, as opposed to Refs. 19 and 20, we consider a field inhomogeneity that is not due to the finite wave number of a free field but to a material inhomogeneity close by. The most simple of such inhomogeneities is the presence of a flat surface nearby. In this section we consider a sphere located at $\vec{r}^{\,d} = (0,0,d)$, a distance d above a flat substrate occupying the $z \leqslant 0$ half-space and illuminated by a plane wave $\vec{E}^{\,i}(\vec{r},t) = \vec{E}^{\,i} e^{i(\vec{k}^i \cdot \vec{r} - \omega t)}$ incident at an angle θ_i with wave vector $\vec{k}^i = (\omega/c)(\sin\theta_i, 0, -\cos\theta_i)$ (see Fig. 1). For convenience and without loss of generality we assume that the incidence plane lies on the x-z plane. Here, $\vec{E}^{\,i} = (\cos\theta_i E^p, -E^s, \sin\theta_i E^p)$ is the amplitude of the incident field, where E^s and E^p denote its s- and p-polarized components. The role of the external field in Eqs. (1) and (2) is played by the local field, $\vec{E}^{\mathrm{loc}}$, defined as

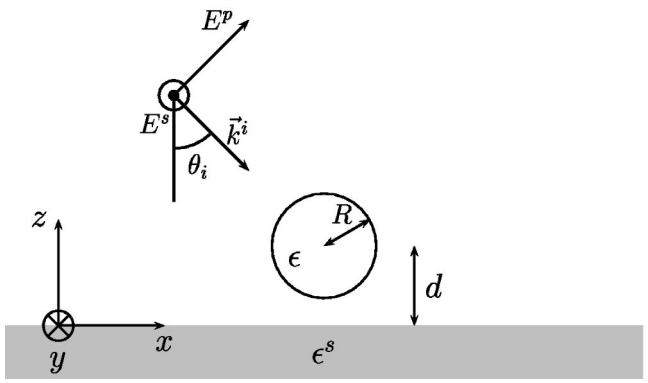

FIG. 1. Sphere of radius R and dielectric function ϵ a distance d above a substrate of dielectric response ϵ^s and illuminated with a plane wave at angle θ_i with s and p contributions.

$$\vec{E}^{\mathrm{loc}} = \vec{E}^M + \overleftrightarrow{T}^I \cdot \vec{p}^{\,l}. \tag{47}$$

The macroscopic field

$$\vec{E}^M = [(1 - r^p)\cos\theta_i E^p, -(1 + r^s)E^s, (1 + r^p)\sin\theta_i E^p] \tag{48}$$

is the nearly homogeneous field that would be present in the absence of the sphere, where r^s and r^p are the Fresnel reflection amplitudes of the substrate for s and p polarizations, respectively.[27] The substrate mediated self-field $\overleftrightarrow{T}^I \cdot \vec{p}^{\,l} = \overleftrightarrow{T} \cdot \vec{p}^{\,I}$ is produced by the image

$$\vec{p}^{\,I} = \frac{1 - \epsilon_1^s}{1 + \epsilon_1^s} \overleftrightarrow{S} \cdot \vec{p}^{\,l}, \tag{49}$$

of the linear dipole

$$\vec{p}^{\,l} = \beta_1^d \vec{E}^{\mathrm{loc}} \tag{50}$$

induced on the sphere, which is located at $\vec{r}^{\,I} = \overleftrightarrow{S} \cdot \vec{r}^{\,d}$, where

$$T_{ij} = \partial_i \partial_j \frac{1}{|\vec{r}^{\,d} - \vec{r}^{\,I}|} \tag{51}$$

is the interaction tensor between two dipoles separated by $\vec{r}^{\,d} - \vec{r}^{\,I} = (0,0,2d)$, while

$$\overleftrightarrow{T}^I \equiv \overleftrightarrow{T} \cdot \overleftrightarrow{S} \frac{1 - \epsilon_1^s}{1 + \epsilon_1^s} \tag{52}$$

is the image-mediated dipolar self-interaction tensor. Here we introduced the dielectric function $\epsilon_m^s \equiv \epsilon^s(m\omega)$ of the substrate. We abbreviate the gradients $\partial_i \equiv \partial/\partial r_i^d$ acting on $\vec{r}^d$ while keeping the position of the image $\vec{r}^I$ constant. $\overleftrightarrow{S} = \mathrm{diag}(1,1,-1)$ is the $z \to -z$ reflection operator, and the linear dipolar polarizability $\beta_m^d = \beta^d(m\omega)$ is given by[27]

$$\beta^d(\omega) = \frac{\epsilon(\omega)-1}{\epsilon(\omega)+2} R^3. \tag{53}$$

According to Eqs. (1) and (2), the nonlinear dipole and quadrupole induced on the sphere by the inhomogeneous local field may be written as

$$p_i' = \chi_{ijk}^d E_j^M E_k^M \tag{54}$$

and

$$Q_{ij}' = \chi_{ijkl}^Q E_k^M E_l^M, \tag{55}$$

where

$$\chi_{ijk}^d = \gamma^d \eta_{lj} \eta_{lik} \tag{56}$$

and

$$\chi_{ijkl}^Q = \frac{1}{2}\gamma^Q \left(\eta_{ik}\eta_{jl} + \eta_{il}\eta_{jk} - \frac{2}{3}\delta_{ij}\eta_{mk}\eta_{ml} \right) \tag{57}$$

represent the nonlinear response of the sphere to the macroscopic field. Here,

$$\eta_{ij} = (\delta_{ij} - T_{ij}^I \beta_1^d)^{-1} \tag{58}$$

is the ''quotient'' between the local and the macroscopic fields, $E_i^{\mathrm{loc}} = \eta_{ij} E_j^M$, and

$$\eta_{ijk} \equiv \partial_i \eta_{jk} = \eta_{jl} T_{ilm}^I \beta_1^d \eta_{mk} \tag{59}$$

with

$$T_{ijk}^I \equiv \partial_i T_{jk}^I = T_{ijl} S_{lk} \frac{1-\epsilon_1^s}{1+\epsilon_1^s} \tag{60}$$

and

$$T_{ijk} = \partial_i T_{jk} = \partial_i \partial_j \partial_k \frac{1}{|\vec{r}^d - \vec{r}^I|}. \tag{61}$$

We have denoted the nonlinear dipole ($\vec{p}\,'$) and quadrupole ($\overleftrightarrow{Q}'$) with a prime in Eqs. (54) and (55) to point out that, even though γ^d and γ^Q given by Eqs. (40) and (41) do incorporate the depolarization effects of an isolated sphere, and that the driving field $\vec{E}^{\mathrm{loc}}$ includes the interaction of the linearly induced dipole at ω with its image, we have not accounted yet for the linear interaction between the dipole and quadrupole moments induced at 2ω and their images ''reflected'' from the substrate. Thus, the total dipole and quadrupole induced at 2ω are given by

$$p_i = p_i' + \beta_2^d \frac{1-\epsilon_2^s}{1+\epsilon_2^s} \left(T_{ij} S_{jk} p_j - \frac{1}{6} T_{ijk} S_{jl} S_{km} Q_{lm} \right), \tag{62}$$

$$Q_{ij} = Q_{ij}' + \beta_2^Q \frac{1-\epsilon_2^s}{1+\epsilon_2^s} \left(T_{ijk} S_{kl} p_l - \frac{1}{6} T_{ijkl} S_{km} S_{ln} Q_{mn} \right), \tag{63}$$

where

$$T_{ijkl} = \partial_i T_{jkl} = \partial_i \partial_j \partial_k \partial_l \frac{1}{|\vec{r}^d - \vec{r}^I|}, \tag{64}$$

and $\beta_m^Q \equiv \beta^Q(m\omega)$ is the quadrupolar linear polarizability, defined as the ratio of the linearly induced quadrupole moment to the gradient of the field, which is given by

$$\beta^Q(\omega) = \frac{\epsilon(\omega)-1}{\epsilon(\omega)+3/2} R^5. \tag{65}$$

As the results for γ^d and γ^Q given by Eqs. (40) and (41) are correct only to order R^3, we should neglect β_2^Q, which is of order R^5 and simplify Eq. (63) to

$$Q_{ij} = Q_{ij}'. \tag{66}$$

Notice that for *s*-polarized incoming light, $\vec{p}$ points along the z direction and $\overleftrightarrow{Q}$ has cylindrical symmetry along the y direction, so that Eq. (62) simplifies to

$$p_z = p_z' - \beta_2^d \frac{1-\epsilon_2^s}{1+\epsilon_2^s} \left(\frac{p_z}{4d^3} + \frac{3Q_{yy}}{64d^4} \right) \quad (s \text{ polarization}). \tag{67}$$

On the other hand, for *p*-polarized incoming light, $p_y = 0$ and $Q_{xy} = Q_{yz} = 0$, so that

$$p_x = p_x' - \beta_2^d \frac{1-\epsilon_2^s}{1+\epsilon_2^s} \left(\frac{p_x}{8d^3} - \frac{Q_{xz}}{16d^4} \right) \quad (p \text{ polarization}), \tag{68}$$

$$p_z = p_z' - \beta_2^d \frac{1-\epsilon_2^s}{1+\epsilon_2^s} \left(\frac{p_z}{4d^3} - \frac{3Q_{zz}}{32d^4} \right) \quad (p \text{ polarization}). \tag{69}$$

Finally, the electromagnetic field radiated above the surface at 2ω may be calculated from Eqs. (42) and (43), but replacing the effective dipole [Eq. (44)] by

$$p_i^{\mathrm{ef}} = \left(p_i - \frac{i}{6} k_2 Q_{ij} \hat{n}_j \right) + \frac{1-\epsilon_2^s}{1+\epsilon_2^s} \left(S_{ik} p_k - \frac{i}{6} k_2 S_{ik} S_{jl} Q_{kl} \hat{n}_j \right), \tag{70}$$

which contains both the electric dipole and the electric quadrupole of the sphere, accounting for the field radiated directly from the sphere towards the observer, and the corresponding image multipoles, which account for the field radiated towards the substrate and then linearly reflected, as illustrated in Fig. 2.

The SH power radiated per unit solid angle is given by Eq. (45) and, since the system is in this case illuminated by a plane wave of amplitude $\vec{E}^i$, we redefine the efficiency [Eq. (46)] as

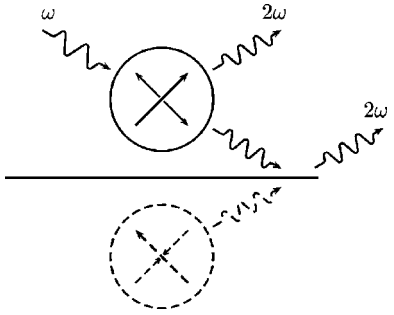

FIG. 2. The SH field radiated by a sphere, illuminated by light of frequency ω (long-wavelength, wiggly line) above a substrate contains direct (solid line) and image (dashed line) dipole (single arrow) and quadrupole (double-headed arrows) contributions (short-wavelength, wiggly lines).

$$\frac{d\sigma}{d\Omega}=\frac{8\pi}{c}k_2^4\frac{|(\hat{n}\times\vec{p}^{\,\mathrm{ef}})\times\hat{n}|^2}{|E^i|^4}. \tag{71}$$

IV. RESULTS

A. Single sphere

To get insight into our results, in Fig. 3 we have plotted the SH radiation pattern $d\sigma/d\Omega$ vs the polar angle θ produced by a dielectric sphere with a dispersionless dielectric function $\epsilon_1=\epsilon_2=2$ and, assuming a frequency-independent a parameter, $a=-2$, and, as is usual for microscopically smooth surfaces, $b=-1$ and $f=0$. Introducing a distance scale $l=|E^{\mathrm{ex}}|/|\nabla E^{\mathrm{ex}}|$ we observe a dipolar pattern for $l=0$ that turns into a quadrupolar pattern as l increases. Both contributions are present when $k_1 l$ is of order one. Notice that, since in this case both $\vec{p}$ and $\overleftrightarrow{Q}$ are real, their contributions to $\vec{p}^{\,\mathrm{ef}}$ are 90° out of phase and therefore no interference between the dipolar and quadrupolar fields is present.

In Ref. 21 a *continuous dipolium* model for a flat homogeneous surface was solved and an explicit expression for the $a(\omega)$ parameter was obtained,

$$a=2([\epsilon_2-\epsilon_1][2\epsilon_1-\epsilon_2-\epsilon_1\epsilon_2] +[\epsilon_1]^2[1-\epsilon_2]\log[\epsilon_1/\epsilon_2])/[\epsilon_2-\epsilon_1]^2, \tag{72}$$

as well as the usual results $b=-1$, $f=0$. To illustrate the analytical structure of the response of a sphere, in Fig. 4 we display the absolute value and the phase of the dipolar response γ^d [Eq. (40)] using the result for the continuous dipolium (72) and a simple Lorentzian dielectric function[28]

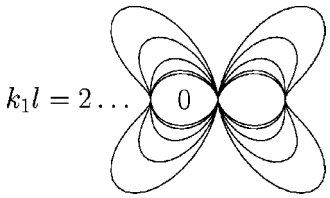

FIG. 3. Normalized SH radiation pattern $d\sigma/d\Omega$ vs θ for a small dispersionless sphere with $\epsilon_1=\epsilon_2=2$ and nonlinear surface parameters $a=-2$, $b=-1$, and $f=0$ illuminated by a field in the z (vertical) direction which varies along z with a characteristic length scale l for different values of $k_1 l$.

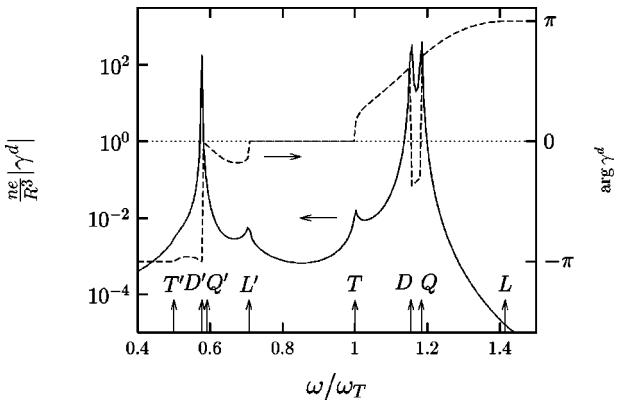

FIG. 4. Absolute value (solid line) and phase (dashed line) of the quadratic dipolar polarizability γ^d of a small sphere with a Lorentzian dielectric function with transverse frequency ω_T and $\omega_L=\sqrt{2}\omega_T$. The small vertical arrows denote the transverse T and longitudinal L frequencies, as well as the dipolar D and quadrupolar Q resonances. The corresponding subharmonics are labeled T', L', D', and Q'.

$\epsilon(\omega)=(\omega_L^2-\omega^2)/(\omega_T^2-\omega^2)$ with transverse and longitudinal frequencies ω_T and ω_L. As discussed in Ref. 21, the imaginary part a'' of a has two broad peaks. One of them extends from $\omega_T/2$ to $\omega_L/2$ and the other from ω_T to ω_L. Its real part a' has peaks at $\omega_T/2$, $\omega_L/2$, and ω_T and a small slope discontinuity at ω_L. The structure of γ^d has features inherited from a. Its phase changes from $-\pi$ to 0 through the region $(\omega_T/2,\omega_L/2)$ and from 0 to π through the region (ω_T,ω_L) and is constant outside of these regions, while its magnitude has a small peak at $\omega_L/2$. However, there is a much larger structure consisting of peaks at the frequencies ω_D and ω_Q of the dipolar and the quadrupolar plasmons of the sphere, given by $\epsilon(\omega_D)=-2$ and $\epsilon(\omega_Q)=-3/2$. There is also a peak at the subharmonic $\omega_D/2$ of the dipolar plasmon, but no structure whatsoever at the subharmonic $\omega_Q/2$ of the quadrupolar plasmon, as discussed above.

In Fig. 5 we show the quadrupolar response γ^Q for the same system as in Fig. 4. As before, we notice structure inherited from that of a between $\omega_T/2$ and $\omega_L/2$ and between ω_T and ω_L, as well as a change in sign slightly above $\omega_L/2$ and an irrelevant 2π phase shift slightly below ω_T. There is also a much larger structure at the dipolar plasmon frequency

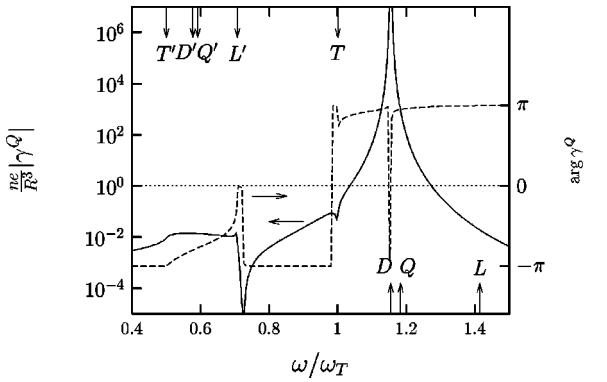

FIG. 5. Absolute value (solid line) and phase (dashed line) of the quadratic quadrupolar polarizability γ^Q of a small sphere. The system and the labels are the same as those in Fig. 4.

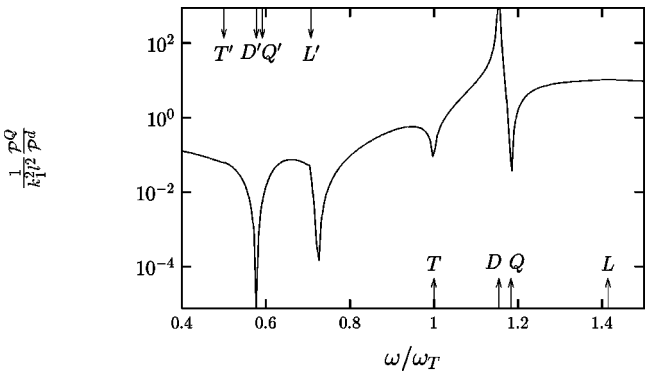

FIG. 6. Ratio of the total quadrupolar $\mathcal{P}^Q$ to the dipolar $\mathcal{P}^d$ radiated power for the same system as in Fig. 4, illuminated by the same field as in 3, normalized to the fundamental wave number k_1 and the length scale of variation of the field l.

ω_D. Notice that as this is a double resonance, the corresponding phase shift across the resonance is 2π. Unlike γ^d, γ^Q has no resonance at the quadrupolar plasmon frequency ω_Q nor at the subharmonics $\omega_D/2$ nor $\omega_Q/2$.

As the frequency dependence of γ^Q differs from that of γ^d, the spectrum of the SH dipolar radiation intensity differs from that of its quadrupolar counterpart. In Fig. 6 we plot the ratio of the total quadrupolar contribution to the radiated power[27] $\mathcal{P}^Q = ck_2^6 \Sigma_{ij} |Q_{ij}|^2/360$ to the total dipolar contribution $\mathcal{P}^d = ck_2^4 |p|^2/3$ for the same system as in Fig. 4, illuminated by a field in the z direction with an inhomogeneity along z with length scale l as in Fig. 3. The figure has a baseline that gradually changes from 10^{-1} to 10^1, so that both contributions are comparable for $k_1 l$ of order one. Superimposed on this baseline, there are additional structures: the slope changes at $\omega_T/2$ and $\omega_L/2$ and the negative peak at ω_T is due to similar structures in the a parameter; the negative peaks at $\omega_D/2$ and ω_Q are due to the dipolar plasmon 2ω resonance and the quadrupolar ω resonance in γ^d, and the negative peak above $\omega_L/2$ is due to the zero in γ^Q. The positive peak at ω_D is due to the dipolar plasmon ω-resonance of γ^Q. Notice that γ^d also has a dipolar plasmon ω-resonance at γ^Q. However, the resonance in γ^d is simple while that of γ^Q is double and therefore dominates [see denominators in Eqs. (40) and (41)].

We remark that, in contrast to the situation in Fig. 3, in general γ^d and γ^Q might differ not only in absolute size but also in phase. For example, a phase difference close to $\pi/2$ may be expected at ω_Q due to the different nature of the resonances, as discussed above. Therefore, in general the SH radiation pattern is not symmetric as in Fig. 3. In Fig. 7 we show schematically the radiation pattern corresponding to a $\pi/2$ phase difference for different values of the length scale l. For small l (large gradient), the radiation pattern is dipolar with its characteristic two lobes. As l increases the angle between the two lobes closes asymmetrically. For even larger l, the quadrupolar radiation dominates for some angles and two new small lobes appear, until, for large enough l symmetry is restored and the typical quadrupolar four-lobed pattern emerges.

B. Si sphere over a dielectric substrate

Recently, SHG experiments have been performed[14] in composite media consisting of Si nanoparticles embedded in a thin-film matrix above a substrate. To explore the nonlinear response of this class of materials, in this section we concentrate on the SH radiation of a single Si nanosphere above a substrate, employing the results of Sec. III. The only quantities required to this end are the bulk linear dielectric response of Si, taken from Ref. 29, its nonlinear surface response a, calculated with Eq. (72), $b=-1$ and $f=0$, and the response of the substrate, which, to simplify the spectra analysis, we take as an inert dielectric with $\epsilon^s = 2.34$.

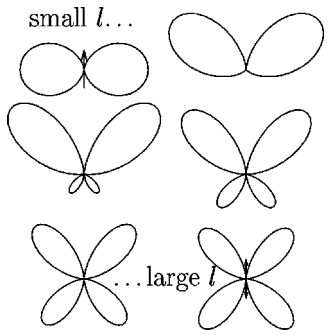

FIG. 7. Schematic radiation patterns $d\sigma/d\Omega$ vs θ for a small dispersionless sphere illuminated by a field as in Fig. 7, assuming a $\pi/2$ phase difference between the dipolar and quadrupolar response, for different values of the field inhomogeneity length scale l, increasing left to right and top to bottom. The direction of the dipole moment is indicated by an arrow and that of the quadrupole moment by a double-headed arrow.

In Fig. 8 we plot the efficiency $d\sigma/d\Omega$ [Eq. (71)] of the SH radiation scattered by a sphere illuminated by s-polarized light as a function of the azimuthal angle φ and of the incoming photon energy $\hbar\omega$. To reduce the simple k_2^4 (k_2^6) dependence of the dipolar (quadrupolar) contributions to $d\sigma/d\Omega$, and to further enhance its structure, we have normalized the results by ω^5. Notice that in this case the SH dipole moment is normal to the surface of the substrate (z axis), while the quadrupole moment has cylindrical symmetry along the normal to the incidence plane (y axis). Thus, the dipolar radiation pattern has cylindrical symmetry around the z axis while there is no quadrupolar radiation along the x-z plane. Therefore, the dipolar and quadrupolar contribu-

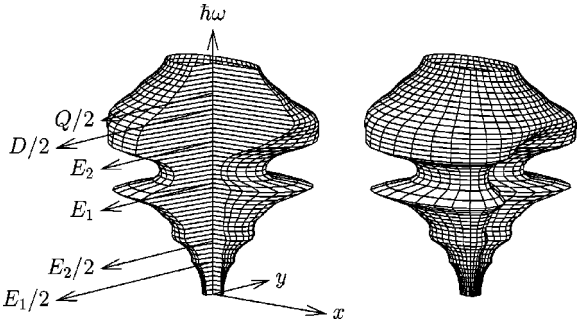

FIG. 8. Normalized SH efficiency $(d\sigma/d\Omega)/\omega^5$ scattered by a Si sphere of radius $R=4$ nm a distance $z=1.2R$ above an inert substrate with $\epsilon^s=2.34$, illuminated with s-polarized light at an angle of incidence $\theta_i=45°$, radiated at a polar angle $\theta=45°$ as a function of the azimuthal angle φ and of the incident photon energy $\hbar\omega$. The plane of incidence is x-z. We indicate the Cartesian axis, the E_1 and E_2 resonances of bulk Si, their subharmonics, and those of the dipolar D and quadrupolar Q resonances of the sphere.

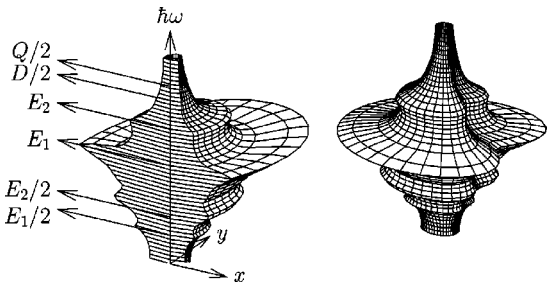

FIG. 9. Normalized SH efficiency $(d\sigma/d\Omega)/\omega^5$ as in Fig. 8, but for *p*-polarized incident light. The sphere is at a distance $z=1.4R$ over the substrate.

tions to the radiation may be extracted from the right and left borders of the 90° cutout in Fig. 8. Following the right border, we notice that the dipolar radiation shows a clear peak close to the critical point $E_1=3.4$ eV of $\epsilon(\omega)$ and a slope change corresponding to $E_2=4.3$ eV. The latter is overshadowed by a large and wide resonance at the subharmonic of the dipolar plasmon of the sphere, at $\hbar\omega_D/2\approx 10$ eV. There are also noticeable features at the subharmonics of the critical points E_1 and E_2. All of these features are present in γ^d [Eq. (40)]. As expected, there is no structure corresponding to the subharmonic of the quadrupolar plasmon of the sphere at $\hbar\omega_Q/2\approx 5.35$ eV. Following now the left border, we find much stronger features at E_1 and E_2 which arise from the quadrupolar response γ^Q [Eq. (41)], as well as the resonances at $E_1/2$, $E_2/2$, and $\hbar\omega_D/2$ also visible on the right border. We remark that the resonance of the quadrupole at E_2 is now comparable to the resonance of the dipole at $\hbar\omega_D/2$.

In Fig. 9 we plot the SH efficiency $d\sigma/d\Omega$ as in Fig. 8, but for *p*-polarized illumination. In contrast to the *s*-polarized case, the direction of the dipole moment $\vec{p}$ is now frequency dependent, and the quadrupole moment $\overleftrightarrow{Q}$ has no axial symmetry. Thus, the dipolar and quadrupolar contributions to the SH radiation cannot be simply identified from the φ dependence of $d\sigma/d\Omega$ (there is, though, a purely dipolar contribution in the grazing direction normal to the incidence plane, $\theta=90°$, $\phi=\pm 90°$ which always correspond to an eigenvector of $\overleftrightarrow{Q}$). Furthermore, there is a clear asymmetry between the SH radiation in the forward $(\varphi=0)$ and the backward $(\varphi=180°)$ directions, as evidenced by the 180° cutout on the left side of Fig. 9. For *p* polarization we found a dipole moment about an order of magnitude larger than for *s* polarization, while the quadrupole moments remain comparable. In order to have similar dipolar and quadrupolar contributions to the radiation we increased *z* from $1.2R$ in Fig. 8 to $1.4R$ in Fig. 9. The latter shows qualitatively the same spectral features as the former ($E_1/2$, $E_2/2$, E_1, and E_2) except for the peak at $\hbar\omega_D/2$ which is hidden by the now much larger peaks at E_1 and E_2 and by our ω^5 normalization.

The full angular dependence of the SH radiation pattern is shown for different distances *d* from the surface in Figs. 10 and 11 corresponding to the cases of *s* and *p* incoming polarizations. For $d=R$ the pattern for *s* polarization (Fig. 10) is dominated by dipolar radiation with the dipole moment normal to the surface; its constant height lines are deformed circles and there is no radiation along the surface normal. As

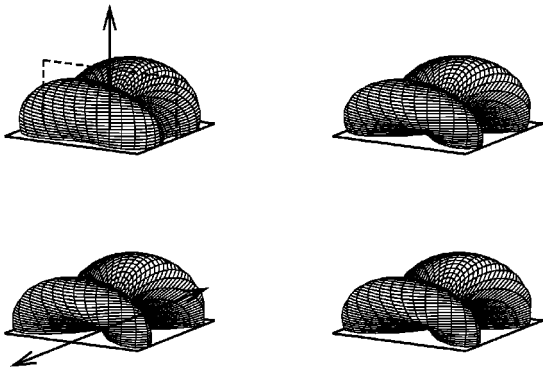

FIG. 10. Efficiency $d\sigma/d\Omega$ of the SH radiation patterns produced by a 4-nm Si nanosphere at several distances $d=1.0R$, $1.2R$, $1.4R$, and $1.6R$ (clockwise from upper left) over a dielectric substrate ($\epsilon^s=2.34$) illuminated by *s*-polarized light of energy $\hbar\omega=E_1$ as a function of the outgoing direction θ and φ. We indicate the surface (solid rectangle), the plane of incidence (dashed rectangle), the direction of the induced dipole moment (single-headed arrow), and the axis of the induced quadrupolar moment (double-headed arrow).

d is increased the relative intensity of the radiation along the incidence plane and along the *y* axis diminishes, and for $d=1.6R$ the typical double-cone pattern corresponding to a cylindrically symmetric quadrupole with axis normal to the incidence plane is clearly seen. On the other hand, for *p* polarization, the pattern is completely dipole dominated for $d=R$, although $\vec{p}$ is slightly tilted from the surface normal. As *d* increases, the radiation pattern acquires peculiar shapes, as the quadrupolar radiation becomes comparable and interferes with the dipolar radiation. We remark that in this case the principal axes of the induced quadrupole are not simply related to the direction of the induced dipole. Furthermore, they are given by complex vectors without a real direction as

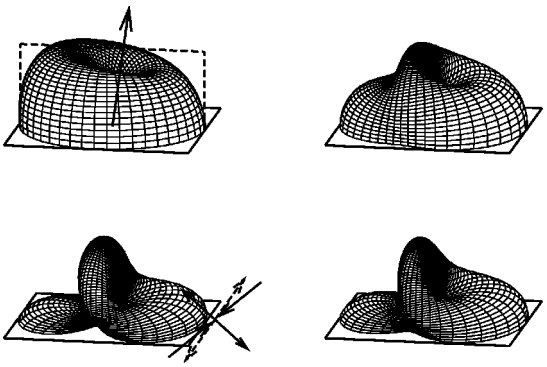

FIG. 11. Efficiency $d\sigma/d\Omega$ of the SH radiation patterns produced by a 4-nm Si nanosphere at several distances $d=1.0R$, $1.4R$, $1.6R$, and $1.8R$ (clockwise from upper left) over a dielectric substrate ($\epsilon^s=2.34$) illuminated by *p*-polarized light of energy $\hbar\omega=E_1$ as a function of the outgoing direction θ and φ. We indicate the surface (solid rectangle) and the plane of incidence (dashed rectangle). For $d=R$ we show the direction of the induced dipole moment (single-headed arrow). For $d=1.8R$ we show with double-headed arrows the approximate principal directions along (solid line) and normal to (dashed line) the incidence plane. Their size indicates that of the corresponding eigenvalues of $\overleftrightarrow{Q}$; converging arrows correspond to nearly opposite phases than diverging arrows.

their real and imaginary parts are not parallel. For $d=1.8R$ the radiation has already become quadrupolar and the quadrupole moment has almost real eigenvectors and almost imaginary eigenvalues, indicated in Fig. 11. In this case the radiation pattern looks like a tilted double cone revolving around the axis with the odd phase, and it is unevenly truncated by the surface of the substrate. The cone is deformed, as the other two principal axes are not equivalent.

V. CONCLUSIONS

In this paper we have obtained analytical expressions for the dipolar and quadrupolar second-order susceptibilities γ^d and γ^Q of a small dielectric sphere in terms of its linear dielectric function ϵ. To this end we employed a continuous dipolium model in which the sphere is considered to be made up of a continuous distribution of polarizable molecules whose density decays to zero abruptly within a thin selvedge at the border of the sphere. We further assumed that the selvedge may be considered locally flat and we neglected finite-size effects. We considered a longitudinal inhomogeneous polarizing field $\vec{E}^{\rm ex}$ and, without further approximations we obtained the leading-order contribution to the dipole moment, proportional to $\vec{E}^{\rm ex}.\nabla\vec{E}^{\rm ex}$, and to the quadrupole moment, proportional to $\vec{E}^{\rm ex}\vec{E}^{\rm ex}$.

We identified surface and bulk contributions to γ^d and γ^Q, and we found that they are all of the same order of magnitude $\approx R^3/(ne)$, where n is the density of polarizable entities within the sphere and e is the electronic charge. Even the surface contributions turn out to be proportional to the volume of the particle $\approx R^3$ and not to its area, where R is the radius. The scattering efficiency is of order $\sigma \approx (R/\lambda)^{6-\zeta}(R/l)^{\zeta}/(cn^2e^2)$ where l is the length scale of the spatial variation of the field, and ζ ranges from 2 for dipole-dominated radiation to 0 for quadrupole dominated radiation. The surface contributions have a resonant structure similar to that of the surface nonlinear susceptibility of a flat semiinfinite system made up of the same material. The bulk contribution to γ^d also has a resonance at the subharmonic of the sphere dipolar plasmon, given by $\epsilon(2\omega)=-2$. Both contributions to γ^d also have resonances at the dipolar plasmon frequency, where $\epsilon(\omega)=-2$ and at the quadrupolar plasmon frequency, where $\epsilon(\omega)=-3/2$. On the other hand, γ^Q displays only an additional feature at the dipolar plasmon frequency, which turns out to be a double resonance.

We have used these results to calculate the SH radiation patterns for an isolated sphere for different length scales l. We obtained a dipolar pattern for small l which evolves continuously into a quadrupolar pattern as l is increased. For kl of order one, both contributions are comparable and the pattern may be symmetric or not, depending on the relative phases of γ^d and γ^Q and the relative orientation of the field and its gradient.

As a realistic application of our theory, we have calculated the SHG of a Si sphere lying above a substrate. In this case, the polarizing field is the local field with a spatially varying contribution arising from the image of the linearly induced dipole moment. We solved this problem self-consistently, accounting also for the images of the second-order dipole and quadrupole moments. For a sphere lying very close to the surface we obtained almost dipolar SH radiation patterns as the system is illuminated with either *s*- or *p*-polarized light. As the sphere is moved away from the surface, the radiation rapidly evolves into a quadrupolar pattern. The patterns are more complex in the case of *p* polarization, since the orientation of the induced moments with respect to the surface and the plane of incidence is less symmetric. An analysis of the azimuthal dependence of the SH radiation intensity shows that for *s* polarization it is feasible to obtain the separate spectral dependence of the dipolar and quadrupolar contributions to the radiation. For *p*-polarized illumination, such separation is not simple. For $\hbar\omega$ between 1 and 6 eV, we found spectral features associated with the bulk critical points E_1 and E_2 of Si, their subharmonics, and the subharmonic of the dipolar plasmon of the sphere.

Although our theory could be extended to incorporate retardation effects and to overcome the long-wavelength assumption, there are many systems of interest, besides those explored in this paper, in which small particles are excited by inhomogeneous fields with small length scales. For instance, ordered or disordered ensembles of spherical particles in two or three dimensions could be fabricated using procedures such as colloidal aggregation, ion implantation followed by thermal annealing, etc. The corresponding polarizing field is then the local field produced partly by neighboring particles and has a length scale of variation of the order of the interparticle distance. We believe that the theory developed in the present paper will prove useful for the understanding of optical nonlinear processes in such complex systems. Even in the simple situations studied here, our results show very rich spectra and nontrivial radiation patterns, whose experimental verification should be pursued.

ACKNOWLEDGMENTS

We acknowledge partial support from Conacyt under Grants Nos. 31120-E (V.L.B.) and 26651-E (B.S.M.), from DGAPA-UNAM under Project No. IN110999 (W.L.M.), and from UBACyT (V.L.B.). V.L.B. is a member of CONICET.

*On leave from Departamento de Física, FCEN-UBA, Argentina.

[1] W. Daum, H.-J. Krause, U. Reichel, and H. Ibach, Phys. Rev. Lett. **71**, 1234 (1993).
[2] J. McGilp, M. Cavanagh, J. Power, and J. O'Mahony, Opt. Eng. (Bellingham) **33**, 3895 (1994).
[3] C. Meyer, G. Lüpke, U. Emmerichs, F. Wolter, H. Kurz, C.H. Bjorkman, and G. Lucovsky, Phys. Rev. Lett. **74**, 3001 (1995).
[4] J.R. Power, J.D. O'Mahony, S. Chandola, and J.F. McGilp, Phys. Rev. Lett. **75**, 1138 (1995).
[5] P. Godefroy, W. de Jong, C.W. van Hasselt, M.A.C. Devillers, and Th. Rasing, Appl. Phys. Lett. **68**, 1981 (1996).
[6] K. Pedersen and P. Morgen, Surf. Sci. **377-379**, 393 (1997).
[7] G. Lüpke, Surf. Sci. Rep. **35**, 75 (1999).
[8] B.S. Mendoza and W.L. Mochán, Phys. Rev. B **53**, 10 473 (1996).
[9] B.S. Mendoza and W.L. Mochán, Phys. Rev. B **55**, 2489 (1997).
[10] P. Guyot-Sionnest, A. Tadjedinne, and A. Liebsch, Phys. Rev. Lett. **64**, 1678 (1990).
[11] B.S. Mendoza, A. Gaggiotti, and R.D. Sole, Phys. Rev. Lett. **81**, 3781 (1998).

[12] D. Lim, M.C. Downer, J.G. Ekerdt, N. Arzate, B. S. Mendoza, V. Gavrilenko, and R. Wu, Phys. Rev. Lett. **84**, 3406 (2000).
[13] B.S. Mendoza, W.L. Mochán, and J.A. Maytorena, Phys. Rev. B **60**, 14 334 (1999).
[14] M. Downer (private communication).
[15] G.S. Agarwall and S.S. Jha, Solid State Commun. **41**, 499 (1982).
[16] X.M. Hua and J.I. Gersten, Phys. Rev. B **33**, 3756 (1986).
[17] D. Östling, P. Stampfli, and K.H. Bennemann, Z. Phys. D: At., Mol. Clusters **28**, 169 (1993).
[18] J. Martorell, R. Vilaseca, and R. Corbalán, Phys. Rev. A **55**, 4520 (1997).
[19] J.I. Dadap, J. Shan, K.B. Eisenthal, and T.F. Heinz, Phys. Rev. Lett. **83**, 4045 (1999).
[20] J.I. Dadap, J. Shan, K.B. Eisenthal, and T.F. Heinz (unpublished).
[21] B.S. Mendoza and W.L. Mochán, Phys. Rev. B **53**, 4999 (1996).
[22] J.A. Maytorena, B.S. Mendoza, and W.L. Mochán, Phys. Rev. B **57**, 2569 (1998).
[23] N. Bloembergen, Rev. Mod. Phys. **54**, 685 (1982).
[24] G. Russakoff, Am. J. Phys. **38**, 1188 (1970).
[25] J. Rudnick and E.A. Stern, Phys. Rev. B **4**, 4274 (1971).
[26] A. Petukhov, V.L. Brudny, W.L. Mochán, J. Maytorena, B.S. Mendoza, and Th. Rasing, Phys. Rev. Lett. **81**, 566 (1998).
[27] J.D. Jackson, *Classical Electrodynamics*, 2nd ed. (John Wiley and Sons, New York, 1975).
[28] N.W. Ashcroft and N.D. Mermin, *Solid State Physics* (Holt, Rinehart and Winston, New York, 1976), Chap. 27.
[29] D.F. Edwards, *Handbook of Optical Constants of Solids*, edited by E. Palik (Academic, New York, 1985), p. 552.